TRANSPORT PHENOMENA IN ZONAL CENTRIFUGE ROTORS

II. A Mathematical Analysis of the Areas of Isodensity Surfaces in Reorienting Gradient Systems

H. W. HSU *and* N. G. ANDERSON

From the Molecular Anatomy Program, Oak Ridge National Laboratory, Oak Ridge, Tennessee 37830. Dr. Hsu's present address is the Department of Chemical and Metallurgical Engineering, The University of Tennessee, Knoxville, Tennessee 37916.

ABSTRACT Zonal centrifuges may be loaded during rotation (dynamically) or at rest (statically). In the latter case, the shearing forces occurring in a liquid confined in a closed cylinder, during the transition from rest to a stable orientation in a high centrifugal force field, were examined qualitatively by evaluating the change of surfaces in each isodense layer. Analytical expressions for isodense surfaces at various levels were obtained as a function of the rotational speeds. Characteristics of the changes of each isodense layer were computed from the formula derived and are presented, in a graphical form, as figures. From these results, an optimal sample-loading location and an ideal control of acceleration or deceleration in a reorienting gradient rotor are concluded.

INTRODUCTION

Zonal centrifugation in a large cylindrical rotor has been developed as a general method for the mass separation of biomaterials ranging in size from whole cells to protein molecules. Most of these methods involve loading and unloading the rotor dynamically (i.e., during rotation). In some instances it is advantageous to load and unload the rotor statically. Such is the case for the isolation of large particles, whole cells, and nuclei, where often very viscous gradient materials are used, and for shear-sensitive materials, such as high molecular weight DNA, which may be damaged by shearing forces in rotating seals. In a previous paper, we have evaluated the velocity and shear-stress distributions for continuous linear gradient solutions (3). The objective of the present study was the qualitative evaluation of the shearing forces between each isodense layer of liquid confined in a closed cylindrical rotor during the transition from rest to a stable orientation, by evaluating the changes of surfaces at various levels as a function of the rotational speeds. Knowledge of shearing forces within a liquid provides us with a guide to the control of rotor acceleration or deceleration in the transition period; such control prevents damage to biomaterial and assures that the separated biomaterial does not remix during the deceleration period. When the cylindrical rotor is rotating at steady state, the liquid in the rotor moves as the elements of a rigid body. Therefore, there is no shearing force caused by the liquid.

STATEMENT OF PROBLEM

We consider a cylindrical rotor system with radius R and height H, shown schematically in Fig. 1 *a*. The rotor is filled, at rest, with density gradient and sample layer. In the figure, the horizontal lines indicate levels or surfaces of equal density in a continuous density gradient. During acceleration, each isodense surface becomes part of a paraboloid of revolution. At a given rotational speed, all isodensity curves are identical, though vertically transposed. Acceleration results in a series of configurations, shown diagrammatically in Fig. 1 (*b* and *c*). At high speed, where the ratio between the centrifugal force and the acceleration due to gravity is very high, the isodense surfaces approach verticality, as shown in Fig. 1 *d*.

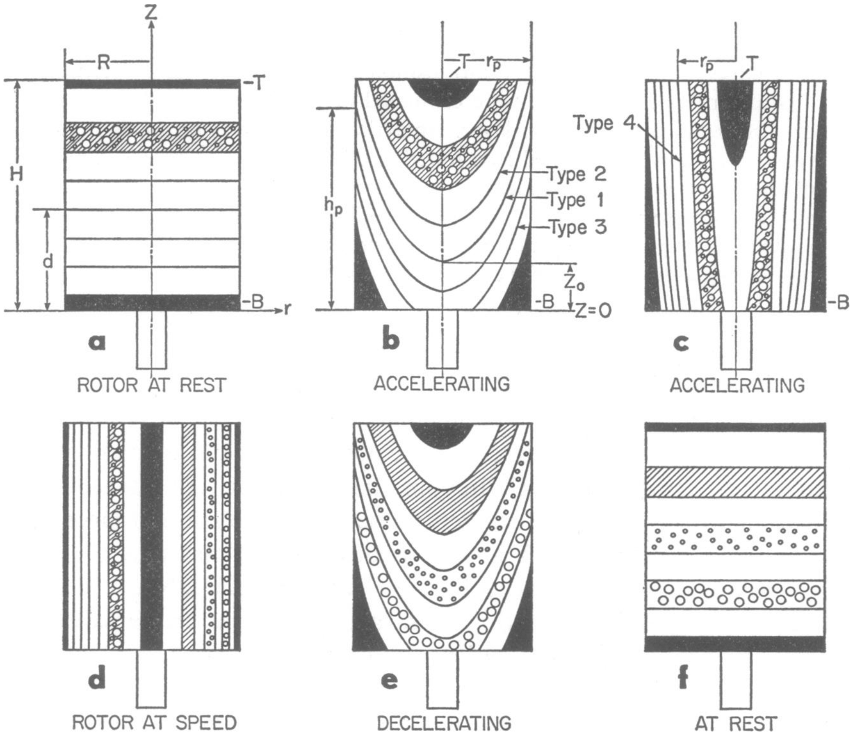

FIGURE 1 Schematic diagram of reorienting gradient rotor system.

Deformations occurring at the various levels may be best understood by describing the changes which occur in layers originally at the top, middle, and bottom of the rotor. The fluid originally against the upper rotor cap becomes squeezed into a small paraboloid of revolution during acceleration (Fig. 1 *b*) and then occupies the center of the rotor at high speed (Fig. 1 *d*). A zone in the middle of the rotor at rest (Fig. 1 *a*) increases in area during acceleration, and then decreases in area slightly as an approximately vertical position is approached. The zone at the very bottom of the rotor at rest (Fig. 1 *a*) decreases markedly in surface area during acceleration (Fig. 1 *b*) but covers the entire surface of the rotor wall at high speed (Fig. 1 *d*). The greatest area changes, therefore, occur in the zones near the top and bottom when at rest, but near the center and the edge at high speed.

The reoriented gradient, before the particles have sedimented appreciably, is shown at the left (Fig. 1 *d*), and after sedimentation at the right. The distribution during deceleration is shown in Fig. 1 *e*, with the distribution at rest shown in Fig. 1 *f*. The separated zones are recovered by draining the gradient out the bottom of the rotor or by displacing it out the top.

MATHEMATICAL ANALYSIS

The equation describing the parabolic surface of revolution is well-known and is given by Bird et al. (2) as

$$z = \frac{\omega^2 r^2}{2g} + z_0 , \tag{1}$$

where z is a vertical axial coordinate, r a radial coordinate as shown in Fig. 1 (*a* and *b*), ω an angular velocity, g gravitational force, and z_0 the minimum of z in the paraboloid, which depends on the angular velocity and the loading level of liquid. The value of z_0 changes from positive to negative with an increase in angular velocity or decrease in loading level, as shown in Fig. 1 *b*. There are four types of paraboloid configurations which will occur, depending on the liquid loading level and change in angular velocity. They are shown in Fig. 1 (*b* and *c*) as 1, 2, 3, and 4;

$$\text{Type 1: } z_0 > 0,\ r_p = R, \quad \text{and} \quad h_p < H,$$

$$\text{Type 2: } z_0 > 0,\ r_p < R, \quad \text{and} \quad h_p = H,$$

$$\text{Type 3: } z_0 < 0,\ r_p = R, \quad \text{and} \quad h_p < H,$$

$$\text{Type 4: } z_0 < 0,\ r_p < R, \quad \text{and} \quad h_p = H,$$

where r_p is the radius of the paraboloid at the rotor wall and h_p the height at the intersection of the paraboloid with the rotor wall.

The interfacial areas of a paraboloid for each type of configuration are obtained as following.

Type 1

The equation describing the paraboloid interfacial area for this configuration is

$$A_1 = 2\pi \int_{z_0}^{h_p} r \left[1 + \left(\frac{dr}{dz} \right)^2 \right]^{1/2} dz. \tag{2}$$

With equation 1,the condition of parabolic surface of revolution, equation 2 is integrated to give

$$A_1 = \frac{2}{3} \frac{\pi g^2}{\omega^4} \left\{ \left[1 + \frac{2\omega^2}{g} (h_p - z_0) \right]^{3/2} - 1 \right\}. \tag{3}$$

The quantities h_p and z_0 in equation 3 are unknown, but they can be evaluated in terms of the liquid volume. The volume of the paraboloid is

$$V = \pi R^2 z_0 + \int_{z_0}^{h_p} \pi (R^2 - r^2)\, dz = \pi R^2 \alpha H, \tag{4}$$

where $\alpha = d/H$ and d is the liquid loading level as shown in Fig. 1 *a*. In equation 4, h_p can be obtained from equation 1, thus

$$h_p = \frac{\omega^2 R^2}{2g} + z_0 . \tag{5}$$

Substituting equation 5 into equation 4, one obtains

$$z_0 = \alpha H - \frac{\omega^2 R^2}{4g} . \tag{6}$$

With equations 5 and 6, the interfacial area of the paraboloid becomes

$$A_1 = \frac{2}{3} \frac{\pi g^2}{\omega^4} \left\{ \left[1 + \frac{\omega^4 R^2}{g^2} \right]^{3/2} - 1 \right\}. \tag{7}$$

Type 2

The interfacial area of a paraboloid of this configuration is

$$A_2 = 2\pi \int_{z_0}^{H} r \left[1 + \left(\frac{dr}{dz} \right)^2 \right]^{1/2} dz. \tag{8}$$

Equation 8 is integrated using the relationship of equation 1, then simplified such that

$$A_2 = \frac{2}{3} \frac{\pi g^2}{\omega^4} \left\{ \left[1 + \frac{2\omega^2}{g} (H - z_0) \right]^{3/2} - 1 \right\}, \tag{9}$$

in which z_0 is the known quantity and can be evaluated in a manner similar to that for type 1:

$$V = \pi R^2 z_0 + \int_{z_0}^{H} \pi(R^2 - r^2)\, dz = \pi R^2 \alpha H. \tag{10}$$

Thus one obtains

$$z_0 = H - R\omega \left[\frac{H(1-\alpha)}{g}\right]^{1/2}. \tag{11}$$

The interfacial radius of the paraboloid at the rotor wall, r_p, can be obtained from equations 1 and 11:

$$r_p = \left\{\frac{2R}{\omega}\,[gH(1-\alpha)]^{1/2}\right\}^{1/2}. \tag{12}$$

Then, the interfacial area for the configuration A_2 becomes

$$A_2 = \frac{2}{3}\frac{\pi g^2}{\omega^4}\left[\left\{1 + \frac{2R\omega^3}{g}\left[\frac{H(1-\alpha)}{g}\right]^{1/2}\right\}^{3/2} - 1\right]. \tag{13}$$

The configuration of the paraboloid becomes type 3 or 4 at high speeds of rotation, where dz/dr is large and the liquid surface is almost vertical, so that the paraboloid is not complete and z_0 is negative. The interfacial area for those types can be obtained by replacing the lower limit of integration of z_0 by zero in equations 2 and 8, and the quantities z_0 and h_p are obtained in the same way as for types 1 and 2. The respective results are:

Type 3

$$A_3 = \frac{2}{3}\frac{\pi g^2}{\omega^4}\left[\left(1 + \frac{\omega^4 R^2}{g^2}\right)^{3/2} - \left\{1 + \frac{\omega^4 R}{g^2}\left[R \pm \frac{2}{\omega}(g\alpha H)^{1/2}\right]\right\}^{3/2}\right] \tag{14}$$

and

$$z_0 = \frac{-1}{2}\frac{\omega^2 R}{g}\left[R \pm \frac{2}{\omega}(g\alpha H)^{1/2}\right]. \tag{15}$$

In equation 15, the selection of sign depends on z_0 and A_3 from the physical situation; that is, negative z_0 and continuity of A_3 in regard to other configurations.

Type 4

$$A_4 = \frac{2}{3}\frac{\pi g^2}{\omega^4}\left[\left\{1 + \frac{\omega^2}{g}\left[H + \frac{\omega^2 R^2}{g}(1-\alpha)\right]\right\}^{3/2} - \left\{1 - \frac{\omega^2}{g}\left[H - \frac{\omega^2 R^2}{g}(1-\alpha)\right]\right\}^{3/2}\right], \tag{16}$$

$$z_0 = \frac{1}{2}\left[H - \frac{\omega^2 R^2}{g}(1-\alpha)\right], \tag{17}$$

and

$$r_p = \left[R^2(1 - \alpha) + \frac{gH}{\omega^2}\right]^{1/2}. \tag{18}$$

If the following reduced variables are defined

$$\frac{\omega^2 R}{g} = \Omega, \qquad \frac{z_0}{R} = \zeta_0, \qquad \frac{r_p}{R} = \rho_p, \tag{19 a, b, c}$$

$$\frac{A_i}{\pi R^2} = S_i, \qquad \frac{H}{R} = \beta, \qquad \frac{d}{H} = \alpha, \tag{19 d, e, f}$$

the above mathematical analysis for the four types of configurations can be summarized below.

Type 1: $0 \leq \zeta_0 < \beta$, $\rho_p = 1$

$$S_1 = \frac{2}{3}\frac{1}{\Omega}[(1 + \Omega^2)^{3/2} - 1] \tag{20}$$

$$\zeta_0 = \alpha\beta - \frac{\Omega}{4} \tag{21}$$

Type 2: $0 \leq \zeta_0 < \beta$, $\rho_p < 1$

$$S_2 = \frac{2}{3}\frac{1}{\Omega^2}[\{1 + 2[\Omega^3\beta(1 - \alpha)]^{1/2}\}^{3/2} - 1] \tag{22}$$

$$\zeta_0 = \beta - [\beta\Omega(1 - \alpha)]^{1/2} \tag{23}$$

$$\rho_p = \left[4\frac{\beta}{\Omega}(1 - \alpha)\right]^{1/4} \tag{24}$$

Type 3: $\zeta_0 < 0$, $\rho_p = 1$

$$S_3 = \frac{2}{3}\frac{1}{\Omega^2}[(1 + \Omega^2)^{3/2} - (1 - 2\zeta_0\Omega)^{3/2}] \tag{25}$$

$$\zeta_0 = -\frac{1}{2}[\Omega \pm 2(\Omega\alpha\beta)^{1/2}] \tag{26}$$

Type 4: $\zeta_0 < 0$, $\rho_p < 1$

$$S_4 = \frac{2}{3}\frac{1}{\Omega^2}\{[1 + \beta\Omega + \Omega^2(1 - \alpha)]^{3/2} - [1 - \beta\Omega + \Omega^2(1 - \alpha)]^{3/2}\} \tag{27}$$

$$\zeta_0 = \frac{1}{2}[\beta - \Omega(1 - \alpha)] \tag{28}$$

$$\rho_p = \left[\frac{\beta}{\Omega} + 1 - \alpha\right]^{1/2} \tag{29}$$

NUMERICAL RESULTS

A FORTRAN program for an IBM 360 series digital computer was written to calculate the paraboloid interfacial area A, the minimum of the paraboloid height z_0, and the interfacial radius of the paraboloid at the rotor wall as a function both of speeds of revolution and the loading levels of liquid. Such calculation permits evaluation of the mathematical results obtained. By use of equations 7, 13, 14, and 16, the paraboloid interfacial area was calculated for A-XVI and K-II rotors; the results are presented in Figs. 2, 3, 4, and 5. The dimensions of these rotors are listed in Table I. The variations of interfacial radius of the paraboloid at the rotor wall were computed from equations 12 and 18 for A-XVI and K-II rotors; the results are given in Figs. 6 and 7. The minima of the paraboloid heights were calculated from equations 6, 11, 15, and 17 for the K-II rotor, and the results are given in Fig. 8.

In order to find an ideal ratio of rotor height to radius, the reduced paraboloid interfacial areas as a function of reduced angular velocity were computed from various values of β at three loading levels, with $\alpha = 0.1$, 0.5, and 0.9 from the derived reduced equations. The results are plotted as Fig. 9.

From Fig. 9 it is found that the reduced interfacial area has fewer variations for $\beta = 0.7$ at $\alpha = 0.5$ (the loading level at the middle of the rotor). Therefore, the

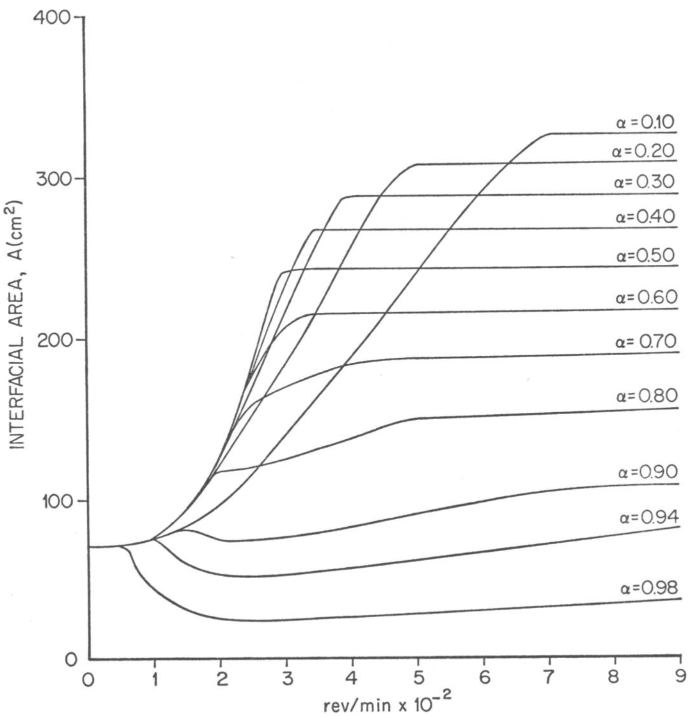

FIGURE 2 Variation of interfacial area with respect to speeds of revolution for A-XVI rotor (0–900 rev/min).

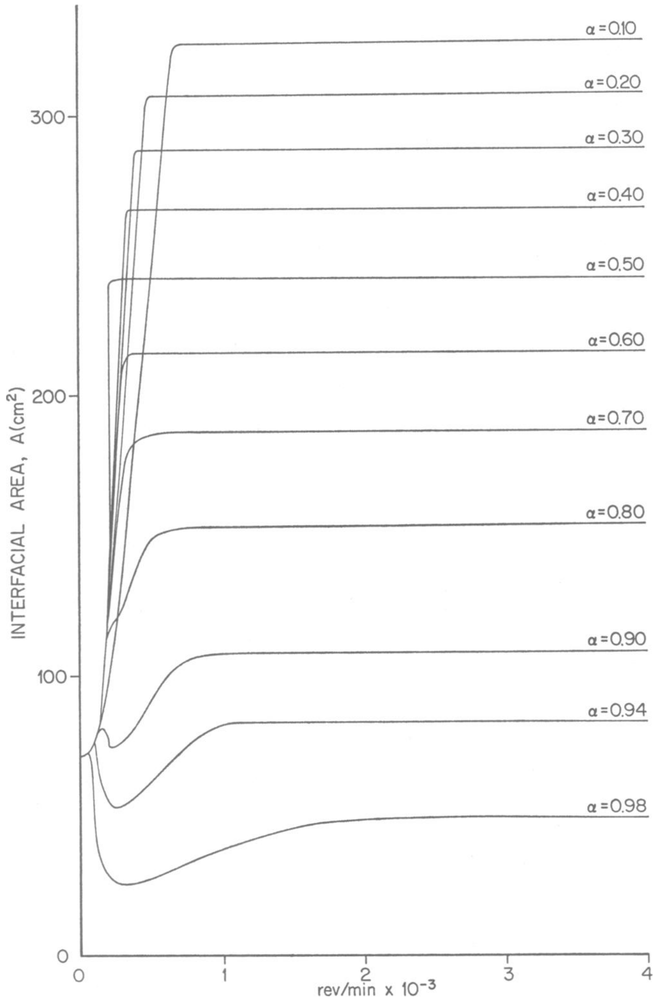

FIGURE 3 Variation of interfacial area with respect to speeds of revolution for A-XVI rotor (0–4000 rev/min).

variations of interfacial area at various loading levels for $\beta = 0.7$ were calculated, and the results are given in Fig. 10. For static loading or unloading, it is preferable to have a rotor with $\beta > 2.0$; the variation of interfacial area for $\beta = 3.0$ is also presented in Fig. 11.

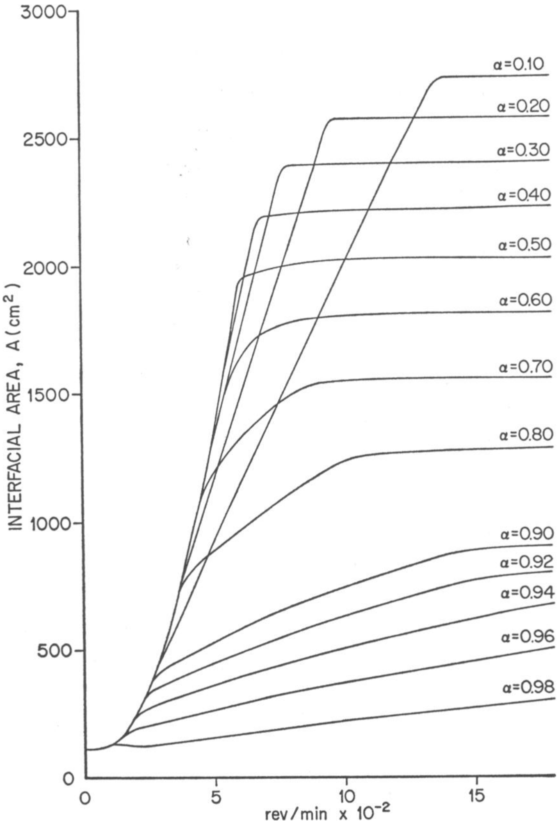

FIGURE 4 Variation of interfacial area with respect to speeds of revolution for K-II rotor (0–1800 rev/min).

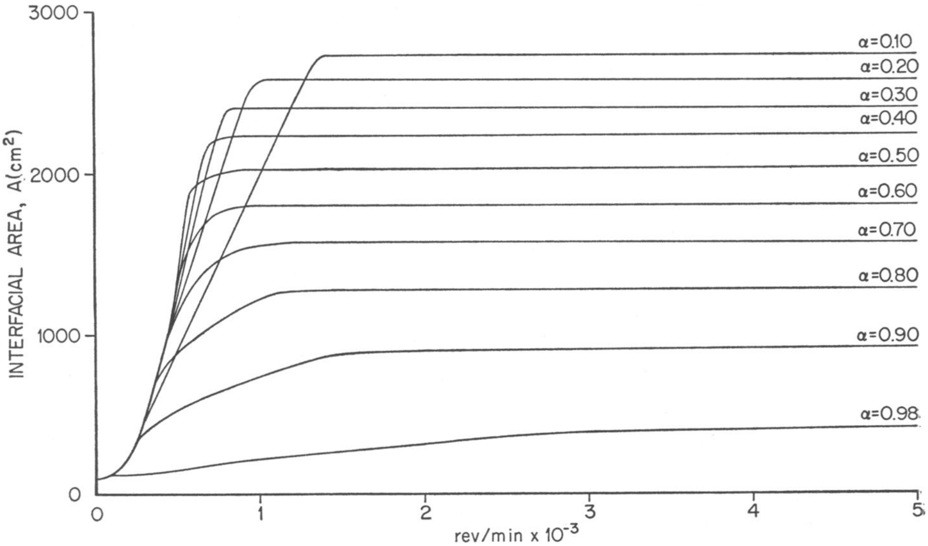

FIGURE 5 Variation of interfacial area with respect to speeds of revolution for K-II rotor (0–5000 rev/min).

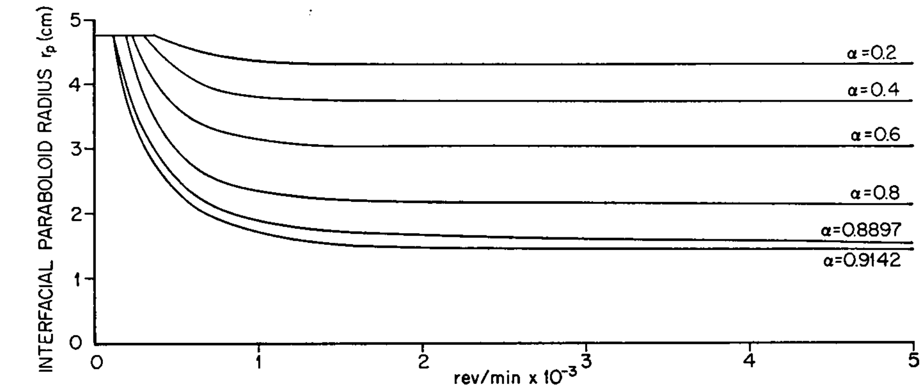

FIGURE 6 Variation of paraboloid interfacial radius with respect to speeds of revolution for A-XVI rotor.

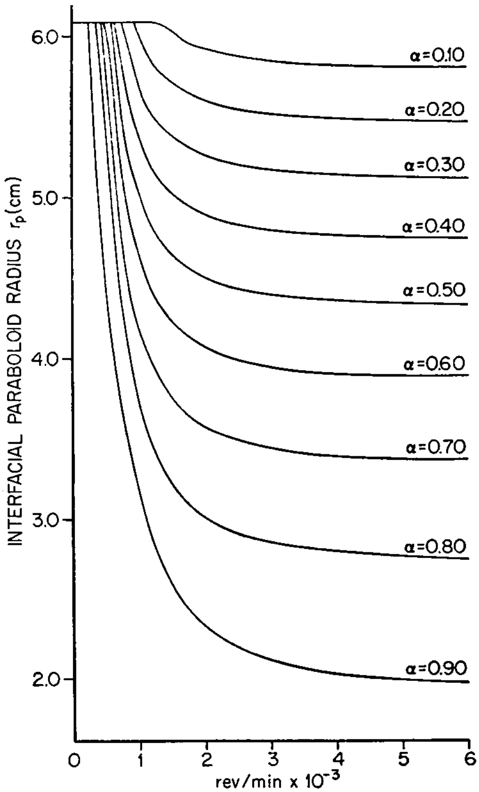

FIGURE 7 Variation of paraboloid interfacial radius with respect to speeds of revolution for K-II rotor.

TABLE I
DIMENSIONS OF ROTORS

	A-XVI	K-II
Diameter, *cm*	9.52	12.19
Height, *cm*	11.47	75.08

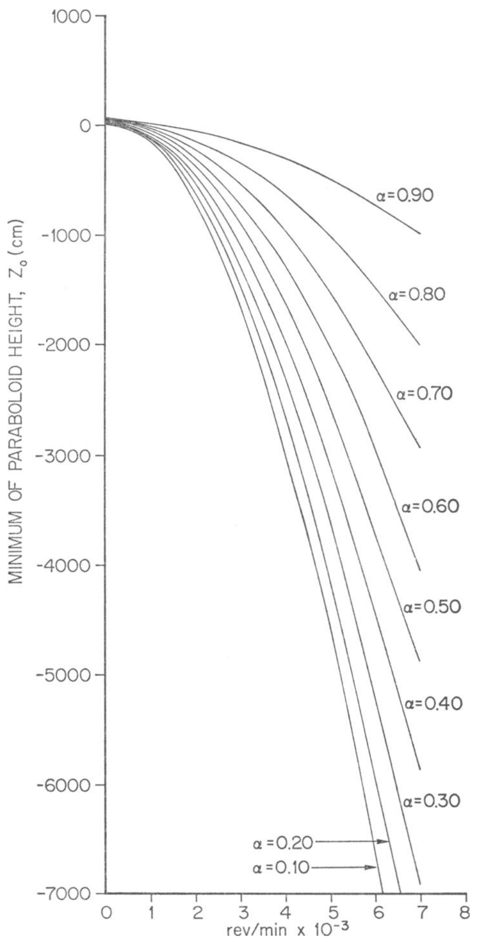

FIGURE 8 Variation of minimum of paraboloid height with respect to speeds of revolution for K-II rotor.

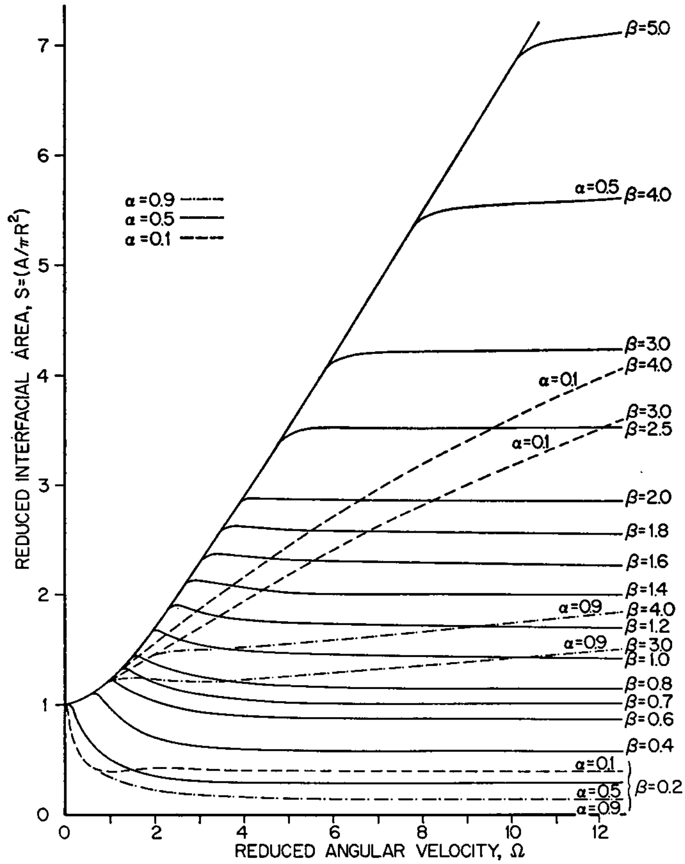

Figure 9 Variation of reduced paraboloid interfacial area with respect to reduced angular velocity for various values of β.

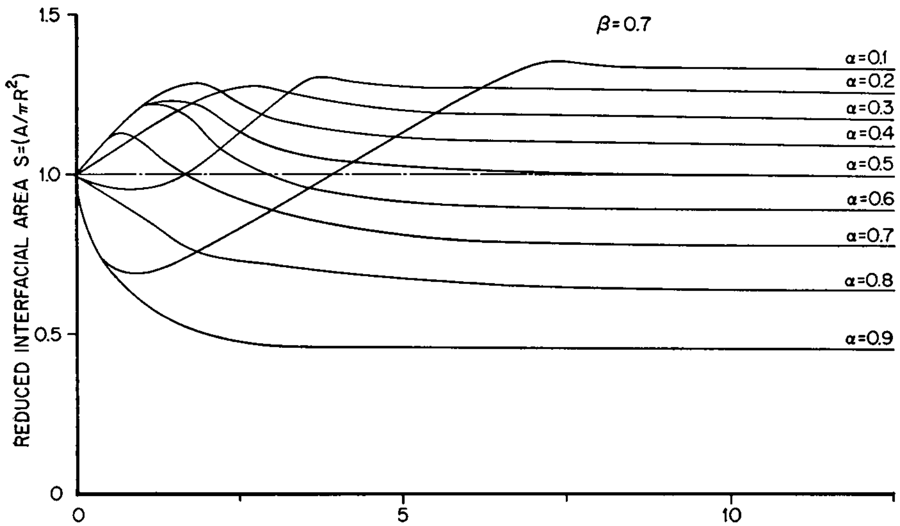

Figure 10 Variation of reduced paraboloid interfacial area with respect to reduced angular velocity for $\beta = 0.7$.

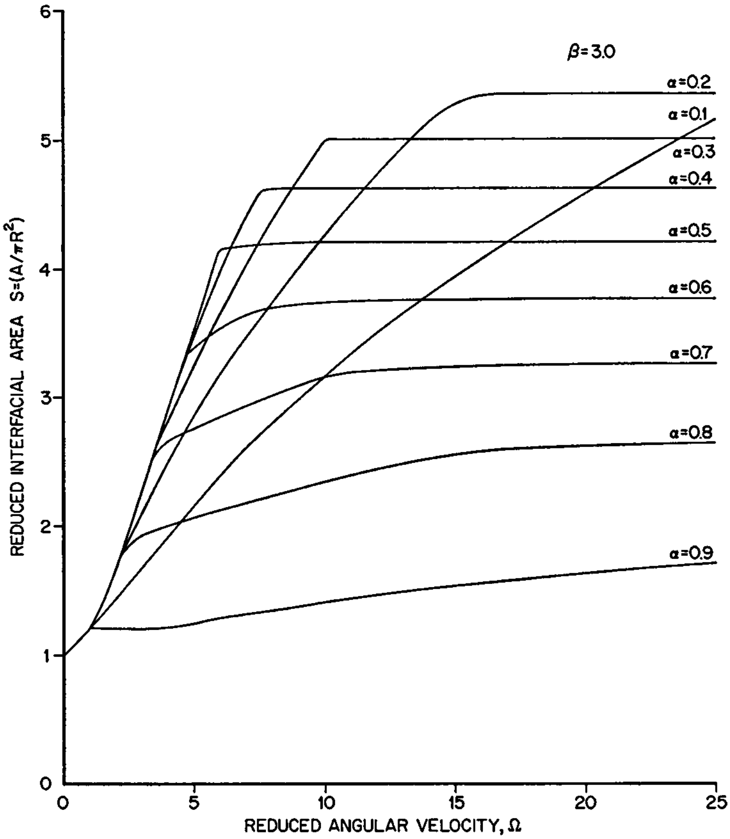

FIGURE 11 Variation of reduced paraboloid interfacial area with respect to reduced angular velocity for $\beta = 3.0$.

DISCUSSION

The results presented here are based on the assumption that the instantaneous steady state is established within a liquid at corresponding speeds of revolution. Therefore, the variations of paraboloid interfacial area, paraboloid interfacial radius at the rotor wall, and the minimum of the paraboloid height investigated are transitions in a series of steady states within a liquid. This is quite different from the transient case. In a thermodynamic sense, a local instantaneous equilibrium is assumed. This assumption is considered reasonable in the qualitative evaluation of the shearing forces between each isodense layer of liquid.

At low speeds of revolution, a mathematical analysis of the areas of isodense surfaces shows that at the lower half of the rotor the rate of change, $dA/d(\text{rev/min})$, increases with the liquid loading level, and at the upper half of the rotor the rate of change decreases with the liquid loading level. In the lower half, the rate of change with respect to the liquid level is positive, and in the upper half it is negative. During an initial period of acceleration, the shear forces which arise from the changes of interfacial area have different directions in the lower and upper halves of a rotor. This difference in direction suggests a turbulence or mixing motion during this period but, because no further variation of interfacial area at each liquid loading level is approached, the turbulence disappears. It is concluded that the start-up period of a rotor control should be as slow as possible. For A-XVI and K-II rotors, the caution speeds are 0–700 and 0–1500 rev/min, respectively. These conclusions can be drawn easily from Figs. 2, 3, 4, and 5.

The magnitude of change is rather small at higher liquid loading levels; therefore, because the shearing force is smaller at higher levels, the sample should load into the rotor as high (near the top) as possible so that the damage to biomaterial will be less. An ideal method of operation is to place a dense "cushion" in the bottom and an overlay of light fluid above the sample layer at the top; the sample layer and density gradient may be restricted to that part of the rotor where the least shearing occurs.

For a zonal centrifuge rotor operating at very low speeds, it is helpful to know the minimum rev/min at which the isodense paraboloid will stop changing its shape with an increase of rev/min. We may define the speeds as a pseudo-steady-state rev/min. From Fig. 8 it is clear that the minimum paraboloid height never approaches a constant value. At high speeds of revolution, the rate of change for z_0 is almost negative infinity, so it is impossible to have no further change in shape of paraboloid with further increasing of rev/min. Therefore, we would like to suggest the use of a paraboloid interfacial area or a paraboloid interfacial radius at the rotor wall as a basis for consideration of a pseudo-steady-state rev/min. If we use a paraboloid interfacial radius at the rotor wall as basis, it will be about 2000 and 5000 rev/min for A-XVI and K-II rotors, respectively. If we choose a paraboloid interfacial area as basis, it also will be about 2000 and 5000 for A-XVI and K-II rotors, respectively.

Reorienting gradient rotors (K-II) are now in commercial use for the production of influenza virus vaccines (4). Further biological applications of the principles are being explored currently at Oak Ridge, including the isolation of serum macroglobulins using the reorienting gradient K-V rotor.

Evaluating an ideal ratio of rotor height to radius, we find from Fig. 9 that if the ratio of rotor height to radius is 0.7, the loading level at the middle of the rotor exhibits the minimum variation of paraboloid interfacial area. This type of rotor, the so-called "FLAT-ROTOR," allows a minimum of mixing within a liquid and thus gives a better resolution. However, with the FLAT-ROTOR a static loading or unloading is rather difficult; so one has to use a dynamic loading or unloading method in charging the sample and gradient solutions into this rotor, which has extra mechanical problems to be solved in design. In the static loading or unloading system, the separated zones are recovered by draining the gradient out the bottom of the rotor or displacing it out the top; therefore, with this system, there are fewer mechanical problems. For "TALL-ROTOR," the ratio equal to 3, the variation of interfacial area is shown in Fig. 11. If one built a 20 cm diameter and 30 cm height rotor, the critical angular velocity for the rotor would be about 15 reduced angular velocity units (from Fig. 11). Thus, from the definition of reduced quantity,

$$\Omega = 15 = R\omega^2/g$$

$$\omega = \left[\frac{\Omega g}{R}\right]^{1/2} = \left[\frac{15 \times 980}{10}\right]^{1/2} = 38.34$$

$$\text{rev/min} = \frac{60 \times \omega}{2\pi} = 366 \sim 370.$$

In practice one has to start the rotor as slowly as possible up to 370 rev/min; then, after this speed is reached, the rate of acceleration of the rotor does not appreciably affect the shearing forces in the liquids.

NOMENCLATURE

A	paraboloid interfacial area [cm^2]
d	liquid loading level [cm]
g	acceleration of gravity [980 cm sec^{-2}]
h_p	height of intersection of isodense paraboloid with rotor wall [cm]
H	height of rotor [cm]
r	radius coordinate
r_p	radius of isodense paraboloid at wall [cm]
R	radius of rotor [cm]
S	reduced paraboloid interfacial area [$= A/\pi R^2$] defined in equation 19 *d*
V	volume of liquid [cm^3]
z	vertical axial coordinate
z_0	minimum of the height of isodense paraboloid [cm]
α	reduced liquid loading level [$= d/H$] defined in equation 19 *f*
β	ratio of rotor height to radius [$= H/R$] defined in equation 19 *e*
ρ_p	reduced radius of isodense paraboloid at wall [$\rho_p = r_p/R$] defined in equation 19 *c*
ζ_0	reduced minimum height of isodense paraboloid [$= z_0/R$] defined in equation 19 *b*
ω	angular velocity [sec^{-1}]
Ω	reduced angular velocity [$= \omega^2 R/g$] defined in equation 19 *a*

Subscripts

0	quantity evaluated at minimum position
1, 2, 3, 4	classification of paraboloid types
P	paraboloid

The initial phase of this work was started by N. G. Anderson and Drs. C. A. Price, W. D. Fisher, R. E. Canning, and C. L. Burger (reference 1). Their work was incorporated in the statement of problem and Fig. 1. The authors wish to express their sincere appreciation to those who contributed to the original idea of this paper and also to acknowledge with thnaks the assistance of Mr. R. A. Carter, who computed the numerical results, and Mr. C. T. Rankin and Mr. L. H. Elrod with whom H. W. Hsu had many valuable discussions during this work.

The Molecular Anatomy Program is supported by the U. S. Atomic Energy Commission, the National Cancer Institute, the National Institute of General Medical Sciences, and the National Institute of Allergy and Infectious Diseases. Oak Ridge National Laboratory is operated for the U. S. Atomic Energy Commission by the Nuclear Division of Union Carbide Corporation.

H. W. Hsu is with the Biology Division, Oak Ridge National Laboratory, as a consultant.

Received for publication 16 July 1968 and in revised form 28 October 1968.

REFERENCES

1. Anderson, N. G., C. A. Price, W. D. Fisher, R. E. Canning, and C. L. Burger. 1964. *Anal. Biochem.* **7**:1.
2. Bird, R. B., W. E. Stewart, and E. N. Lightfoot. 1960. Transport Phenomena. McGraw-Hill Book Co., New York. 98.
3. Hsu, H. W. 1968. *Biophys. J.* **8**:973.
4. Reimer, C. B., R. S. Baker, R. M. Van Frank, T. E. Newlin, G. B. Cline, and N. G. Anderson. 1967. *J. Virol.* **6**:1207.